Available online at www.sciencedirect.com

ScienceDirect

Procedia CIRP 33 (2015) 376 – 381

www.elsevier.com/locate/procedia

9th CIRP Conference on Intelligent Computation in Manufacturing Engineering - CIRP ICME '14

Modelling of the crater formation in micro-EDM

Bai Shao[a], Kamlakar P. Rajurkar[a,]*

[a]*University of Nebarska Lincoln, 1400 R Street, Lincoln NE 68588, U.S.A.*

* Corresponding author. Tel.: +1-402-472-0454 ; fax: +1-402-472-1465. *E-mail address:* krajurkar1@unl.edu

Abstract

A comprehensive electro-thermal model of micro-EDM has been used to simulate the crater formation process is presented. This model incorporates realistic machining conditions such as Gaussian distributed heat flux, temperature dependent thermal properties and expending plasma radius. The heat transfer equation and experimental measurements of a generated crater dimensions are used to determine the energy distribution fraction to the electrodes, a crucial parameter of the micro-EDM modelling. Simulation results show a good agreement with experimental results.

Selection and peer-review under responsibility of the International Scientific Committee of "9th CIRP ICME Conference"

Keywords: EDM; Modelling; FEM

1. Introduction

Electrical Discharge Machining (EDM) process removes material by a series of electric sparks between two electrodes submerged in the dielectric fluid such as hydrocarbon oil. The non-contact erosion mechanism of EDM can machine electrically conductive materials regardless of their hardness. Micro-EDM produces micro features with high accuracy and precision. These unique advantages make EDM and micro-EDM suitable to manufacture complex shaped dies and critical parts required in automobile, aerospace, and medical industries [1].

EDM is a complex and stochastic process and involves many mechanisms such as electrodynamics, electromagnetic, thermodynamic, and hydrodynamic [2]. A very small gap in micro-EDM poses additional challenges in understanding and modelling the process. It is necessary to develop quantitative expressions or models to predict the process performance parameters such as material removal rate (MRR), tool wear ratio (TWR) and surface roughness (SR). Many attempts of developing thermal models have been reported in EDM literature since 1971 [3]. In general, researchers attempted to develop models and their solution using simplified geometry and boundary conditions [4,5]. In most of these cases the prediction error of these models was found to be very large due to simplified assumptions and conditions. Moreover, the re-solidification was not account for which is difficult to mathematically incorporate into modeling process. It is expected that inclusion of accurate parameters and realistic conditions such as expanding heat source, and temperature dependent thermal physical properties will improve the prediction of performance parameters. The analytical solution with these conditions needs numerical methods such as Finite Element Method (FEM). The use of FEM software, and incorporating realistic working conditions, the EDM and micro-EDM process can be improved for better prediction [6–8].

The material removal mechanism in EDM and micro-EDM is not fully understood but more and more recent studies indicate that the existing EDM electro-thermal models also can be applied to the micro-EDM process [6,8–10]. A comprehensive thermal model with Gaussians distributed heat flux, temperature dependent thermal properties, expending plasma radius and experimentally determined energy distribution fraction has been developed and solved by using the FEM technique. This model has been verified by comparing the simulation results with the experimental measurements. The second section describes micro-EDM

Selection and peer-review under responsibility of the International Scientific Committee of "9th CIRP ICME Conference"
doi:10.1016/j.procir.2015.06.085

thermal model. The determination of energy distribution along with experimental details is explained in section three. Section four presents simulation results and related analysis. Conclusions of this paper are given in section five,

2. Micro-EDM thermal model

In the EDM process, the plasma channel forms after the breakdown occurs between anode and cathode at the beginning of the discharge. A very high intensity current flows through the plasma channel heating both electrodes. The molten and vaporized material is ejected out at the end of on-time. A crater is left after each discharge. In the micro-EDM a similar phenomenon is believed to happen only at a much smaller gap and during a much shorter time but with a higher energy density.

To develop a micro-EDM thermal model, following assumptions are generally made:

- Only one plasma channel will be formed for each discharge.
- Pulse energy is only contributed by the current and voltage.
- Pulse energy distribution is constant during discharge process.
- Pulse energy distributed into the electrode only by conduction heat transfer.
- The heat loss due to radiation and material removal are neglected.
- The electrode material is homogeneous and isotropic.
- Molten material is removed after each discharge.

Fig. 1. shows a general micro-EDM model by considering only the heat transfer within the material. The electrodynamics, electromagnetic, and hydrodynamic phenomena in the process are not considered. In the model, the plasma channel is considered as a disc heat source with a radius of r_p and its heat flux is q_0. The boundary conditions are insulation by the side and bottom surface and convection on liquid solid interface. By assuming that all the molten and vaporized materials are removed after the discharge, the crater geometry can be estimated by the melting isothermal.

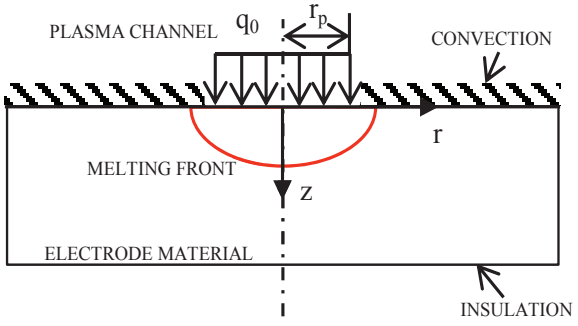

Fig. 1. schematic diagram of the micro-EDM model.

This heat transfer model is given by

$$\frac{1}{r}\frac{\partial}{\partial r}\left(r\frac{\partial T}{\partial r}\right)+\frac{\partial^2 T}{\partial z^2}=\frac{1}{\alpha}\frac{\partial T}{\partial t} \quad (1)$$

the boundary conditions are

$$-k\frac{\partial T(r,0,t)}{\partial z}=\begin{cases}q_0(r,t) \text{ for } 0<r<r_p(t)\\ h(T_r-T) \quad \text{for } r>r_p(t)\end{cases} \quad (2)$$

$$\frac{\partial T}{\partial r}=0, at\ r=R \quad (3)$$

$$\frac{\partial T}{\partial z}=0, at\ r=Z \quad (4)$$

and the initial condition is

$$T(r,z,0)=T_r \quad (5)$$

In Eq. (1-5), r and z are radius and depth in cylindrical coordinates; T is the temperature; T_r is the room temperature; α is the diffusivity; k is the thermal conductivity; h is the heat transfer coefficient; r_p is the plasma radius and q_0 is the heat flux.

The analytical solutions of Eq. (1) with assumptions such as constant thermal physical properties, fixed plasma radius and uniform distributed heat flux, have been found in [11]. However, the model prediction does not match experimental results. Some experimental observations have led to questions about the uniform distributed heat flux and fixed plasma radius assumptions [12].

The model used in this study replaces the fixed radius heat source with an expanding heat source. The expanding rate is shown in Eq. (6),

$$r_p(t)=0.788*t^{0.75}\ [5] \quad (6)$$

Additionally, Gaussian distributed heat flux is used to replacing the uniform heat flux,

$$q_0(r,t)=3.1572\frac{CQ}{\pi r_p(t)^2}exp\left[-3\left(\frac{r}{r_p(t)}\right)^2\right]\ [8] \quad (7)$$

where Q is discharge energy, and C is the energy fraction distributed in to the electrode. And temperature dependent thermal properties are also applied. A recent study shows that this model have a better results than others [13].

3. Parameter determination

The accuracy of model prediction are highly depends on the accuracy of parameters such as plasma radius and energy distribution. Previous methods for determining the energy distribution are based on the temperature rise of the electrodes [14,15]. The experimental method involves special equipment and is difficult to apply in micro-EDM.

An analytical method to address this problem is reported in [16]. This method solves the heat transfer equation reversely and gets the value of the energy distribution ratio and the plasma radius.

3.1. Analytical method to identify the energy distribution to the electrodes and plasma radius

The analytical solutions of the semi-infinite body with constant uniform heat flux model is given below,

$$\frac{T(r,0,t)}{q_0 r_p/k} = \int_{\beta=0}^{\infty} \mathrm{erf}\left[\frac{\beta(\alpha t)^{1/2}}{r_p}\right] J_0\left(\frac{\beta r}{r_p}\right) J_1(\beta)\frac{d\beta}{\beta} \quad (8)$$

$$\frac{T(0,z,t)}{q_0 r_p/k} = \frac{2\sqrt{\alpha t}}{r_p}\left[\mathrm{ierf}\left(\frac{z}{2\sqrt{\alpha t}}\right) - \mathrm{ierf}\left(\frac{\sqrt{z^2+r_p^2}}{2\sqrt{\alpha t}}\right)\right] \quad (9)$$

where J_0 and J_1 are the Bessel functions of the zero and first order; *ierf* is the inverse error function; q_0 is the heat flux can be acquired by the measurement data of the oscilloscope by using the equations given below,

$$Q = \frac{1}{t_{on}}\sum_{t=0}^{n} V(t)I(t)\Delta t \quad (10)$$

$$\mathrm{q}_0(t) = \frac{CQ}{\pi {r_p}^2} \quad (11)$$

where Q is the average discharge energy of the plasma, $V(t)$ and $I(t)$ are time series data of voltage and current, Δt is the sampling interval, t_{on} is pulse on time, and C is the energy distribution fraction to the electrode.

Assuming that the crater is formed by the removal of all the molten materials, therefore the crater radius r_m and depth z_m are points where the temperature reaches the melting point at the end of the discharge. The energy distribution fraction C can be solved by substituting the measured r_m and z_m back to (8) and (9).

Table 1. Experimental parameters

Workpiece	: #304 stainless steel
Tool electrode	: ø100μm tungsten wire
Dielectric	: Kerosene
Power supply	: RC circuit
Open circuit voltage	: 60V, 90V, 120V
Capacitance	: 220pf, 3300pf
Workpiece polarity	: +, -

3.2. Experimental setup

The experiments are conducted on Panasonic MG-ED72W micro-EDM machine. Tektronix TPS 2024 oscilloscope (2GHz sampling rate per channel) is used to record the discharge voltage and current data. Tektronix CT-2 current probe is applied. The Vecco Digital Instruments Dimension 3100 SPM system is used to measure the dimensions of the craters. Experimental parameters and conditions are listed in Table 1.

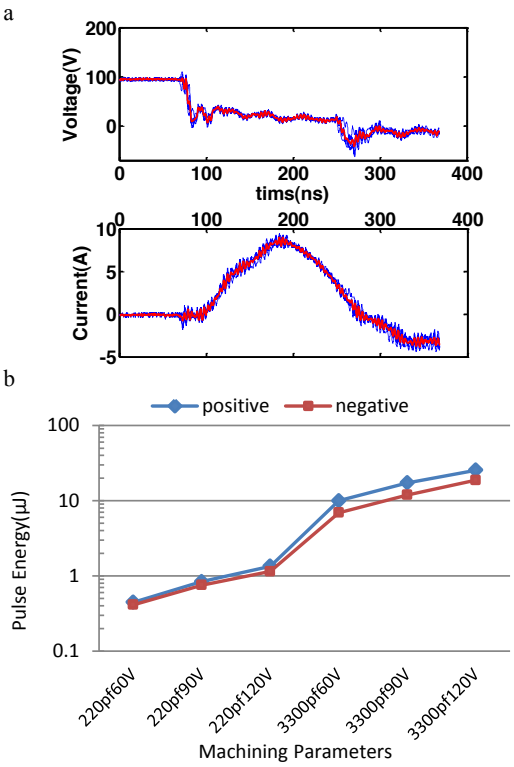

Fig. 2. (a) voltage and current waveforms (3300pf, 90V, positive); (b) pulse energy in different machining conditions.

3.3. Measurement

3.3.1. Discharge energy measurement

Fig. 2. (a) is a representative picture of the current and voltage waveforms, measured by the oscilloscope with the machining condition of 3300pf capacitance, 90V open voltage and workpiece positive polarity. The blue dash lines in the picture are five times individually acquired data stacked together. The data is aligned by the trigger point, and the picture shows a high repeatability. The red solid lines are the average value of each sampling point, which are used as input in the simulation. Fig. 2. (b) shows the average pulse energy for all the machining conditions. The pulse energy increases with the increasing of open voltage and capacitance. The pulse energy is lower when the workpiece is set as negative polarity than it is set as positive. It may due to the difference materials and geometries are used for the workpiece and tool electrodes.

3.3.2. Crater Geometry measurement

Fig. 3. shows a crater generated with the same machining condition measured by AFM. Fig. 3.(a) is the 3D profile of

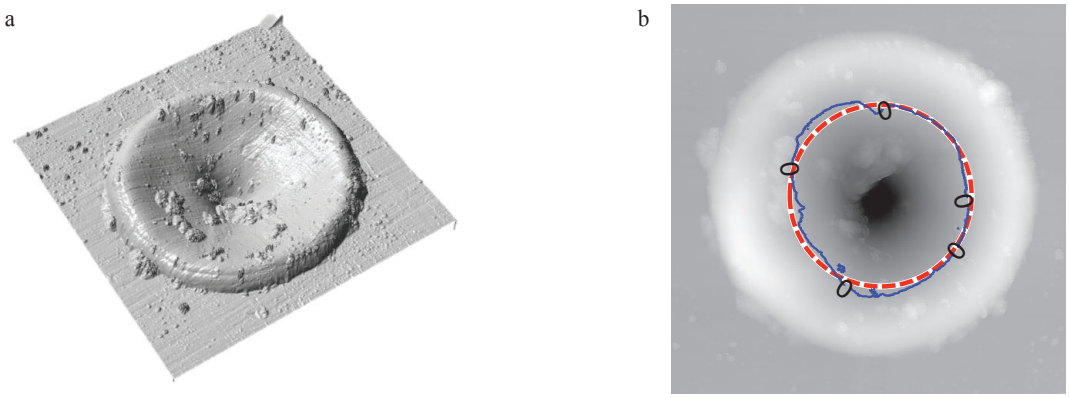

Fig. 3. (a) 3D crater profile; (b) crater grayscale picture. (3300pf, 90V, positive)

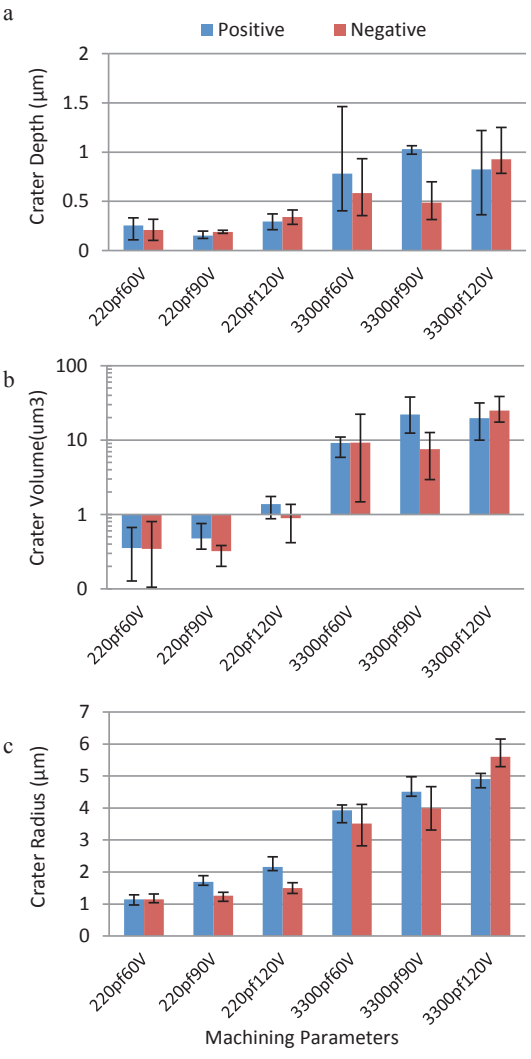

Fig. 4. (a) measured crater depth; (b) measured crater volume (c) measured crater radius.

a bowl shape crater geometry. However, the depth and radius of the crater cannot be measured directly. It takes several steps to get these values. First, fit the un-machined surface with a plane as reference plane. Second, subtract the scanned surface by the reference plane to compensate the tilt and adjust the height value. Then, the residual of the subtraction is the crater geometry with actual height value. Then, the depth of the lowest point in the crater is taken as crater depth. The volume of the crater is the summation of the height times the scanning resolution within the machining area. Fig. 3. (b) shows the how the crater radius is measured. In the picture, the brightness represents the height, the brighter the higher. The blue solid line is the zero height contour, and the red dash line is the circle fits the contour. The radius of the circle is taken as the crater radius.

Fig.4 (a-c) show the measured crater depth, crater volume and crater radius. At least 3 craters are measured for each machining condition. In Fig. 4. (a), it shows that the crater is deeper for the larger capacitance, which is because the pulse energy is 20 times higher than the smaller capacitance, so the crater depth is deeper. With the same capacitance, the pulse energy of 120V open voltage is 3 times larger than the 60V open voltage. But the crater depth is not increasing with the increase of the open voltage. Fig. 4. (b) shows the crater volume which is the removal amount of a single discharge. The volume increases with the increase of the pulse energy. In Fig. 4. (c), the crater radius is bigger with larger capacitance and higher open voltage. It is due to the higher of pulse energy and larger plasma radius.

3.4. Results

By solving Eq. (8) and (9) with the experimentally collected crater radius and depth, the pulse energy distribution ratio and the plasma radius can be obtained for the simulation. Fig. 5 shows the pulse energy distribution. The average fraction of pulse energy distributed to the anode is 7.37%, and to the cathode is 6.78%. In most machining conditions, the ratios of the total energy to the anode are higher than the ratios to the cathode. But, with the machining condition of 3300pf capacitance and 120V open voltage, the pulse

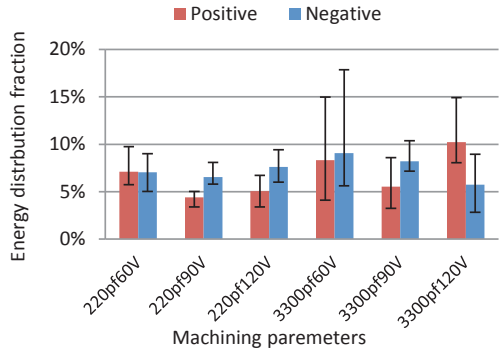

Fig. 5. energy distribution.

energy distributed to the cathode is significantly more than it is distributed to the anode. The reason of this dramatic change has not been found yet.

4. FEM simulation and analysis

4.1. Simulation

By applying the realistic boundary and physical conditions, which are Gaussian distributed heat flux, temperature dependent thermal properties and expanding plasma radius, to the heat transfer model, the mathematical description of the model becomes very complex, FEM has to be used to solve the problem. Commercial FEM software COMSOL is used in this study.

In the FEM simulation, experimentally obtained parameters have been input into the model, such as discharge energy, energy distribution fraction, and pulse on time. The temperature dependent thermal properties [17] and melting latent heat are also applied.

Fig. 6. (a) shows the simulated temperature distribution within the workpiece, as well as the melting isothermal, with the machining condition of 3300pf, 90V and positive polarity. The melting isothermal profile is deeper inside and shallower outside. It is because the expanding of the heat source. The energy is more concentrated at the beginning when the radius is small so it is deeper inside. But the outside surface has less heating time, it is shallower. Fig. 6. (b) compares the simulated melting isothermal to the actual crater profiles. The radius of the simulation is close to the experiments, but the simulation overestimate the depth of the crater. It is because not all the molten materials have been removed after the discharge. The unremoved molten material will re-solidify and forms a recast layer after the discharge.

The simulation result can be further improved by considering the re-solidification of the unremoved molten material. The depth of the simulation can be adjusted by a scaling factor z_e/z_s, where z_e is the measured experimental crater depth, and z_s is the simulation crater depth. The difference between the adjusted simulation and the origin simulation can be considered as the recast layer. The red line in Fig. 6. (b) shows an adjusted simulation, which fits the measurements better. The area between the simulation and the adjusted simulation is the recast layer.

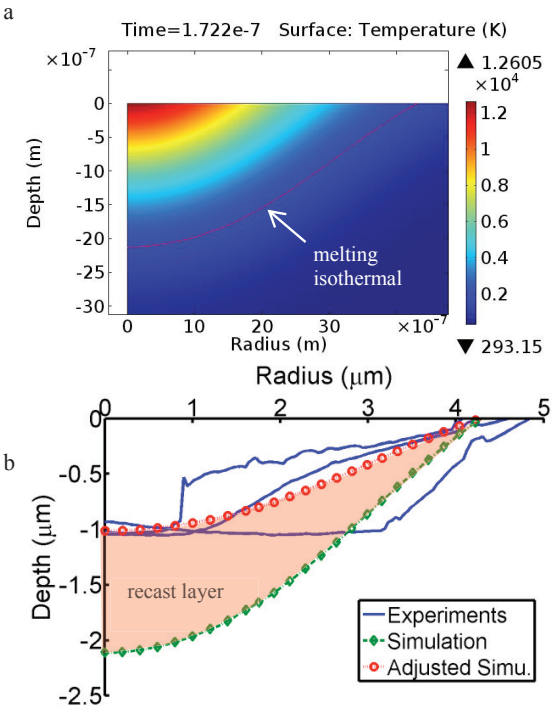

Fig. 6. (a) temperature distribution; (b) experiments V.S. simulation. (3300pf, 90V, positive)

4.2. Results and analysis

Fig. 7 compares the simulated depth, radius and crater volume to the experimental measurements. In Fig. 7.(a) the simulated depths are significantly deeper than the measurements. The average scaling factor is 40%, which means only 40% of the molten material will be considered as removed in simulation. By times the average scaling factor to the simulations, the adjusted depth values are closer to the experimental measurements.

Fig. 7. (b) compares the simulated and measured radius. Generally, the simulations are smaller than the measurements, and the average error is -11%, which is a very good estimation compares to other models [11]. The error of the crater radius may be reduced by applying a more accurate plasma radius expanding model.

The crater volumes are compared in Fig. 7. (c). The simulation results are far overestimated the crater volume without adjustment. After considering the re-solidification and applying the adjustment scaling factor to the simulation results, the estimated errors have been significantly reduced. The average estimated volume error is only 27%. However, some estimation errors are more than 50%. The reason for the large errors is due to the small sample size. Because under some machining conditions, the AFM pictures show the shape of re-solid molten droplets in the crater, the craters shape are as ideal bowl as it shows in Fig. 3. (a). The exist of the re-solid droplets will cause the measured crater volume much smaller than the average, which leads to large errors.

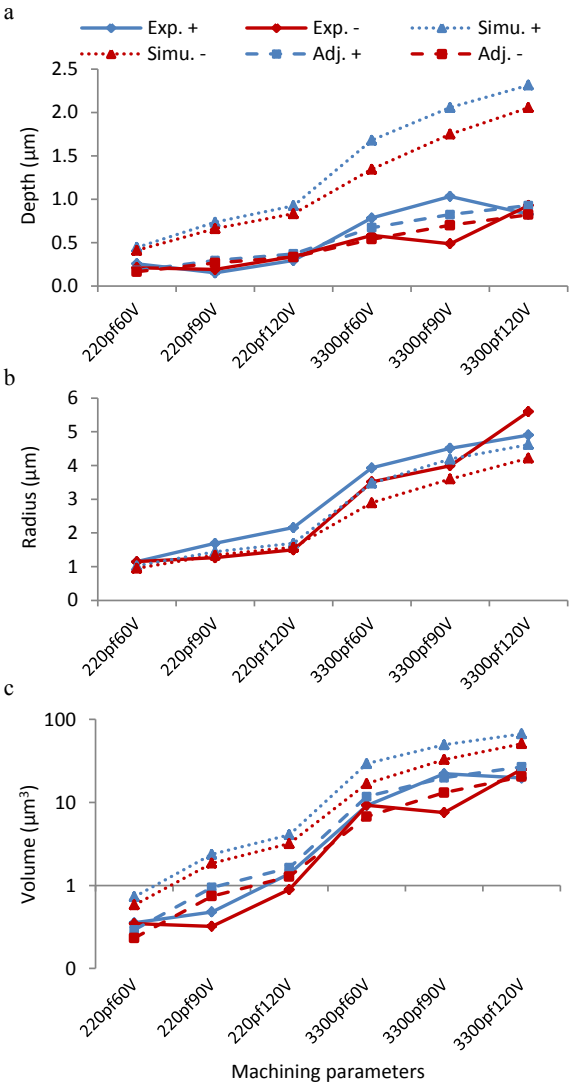

Fig. 7. compare of the simulation and adjusted simulation (a) depth; (b) radius; (c) volume.to the experiments

5. Conclusion

In this paper, a comprehensive electro-thermal model of micro-EDM has been used to simulate the crater formation process. This model incorporates realistic machining conditions such as Gaussian distributed heat flux, temperature dependent thermal properties and expending plasma radius. Experimentally determined parameters such as pulse energy, pulse on time and energy distribution fraction has been applied in the model and solved by using the FEM.

The heat transfer equation and experimental measurements of a generated crater dimensions are used to determine the energy distribution fraction to the electrodes, a crucial parameter of the micro-EDM modelling. The determined pulse energy distributed to the anode is 7.37%, and to the cathode is 6.78%.

Simulation with consideration of the re-solidification in the crater formation process gives close results of the crater geometry. And the average error of the crater radius is -11%, and of the cater volume is 27%.

Acknowledgements

The partial support from NSF Award #1317361 is acknowledged.

References

[1] Rajurkar KP, Levy G, Malshe A., Sundaram MM, McGeough J, Hu X, et al. Micro and Nano Machining by Electro-Physical and Chemical Processes. CIRP Ann - Manuf Technol 2006;55:643–66.

[2] Boothroyd G, Winston A. Fundamentals of machining and machine tools. vol. 198. third. CRC Press; 2006.

[3] Snoeys R, Van Dijck FS. Investigation of electro discharge machining operations by means of thermo-mathematical model. CIRP Ann 1971;20:35–7.

[4] DiBitonto DD, Eubank PT, Patel MR, Barrufet MA. Theoretical models of the electrical discharge machining process. I. A simple cathode erosion model. J Appl Phys 1989;66:4095–103.

[5] Patel MR, Barrufet MA, Eubank PT, DiBitonto DD. Theoretical models of the electrical discharge machining process. II. The anode erosion model. J Appl Phys 1989;66:4104–11.

[6] Tao J, Ni J, Shih AJ. Modeling of the anode crater formation in electrical discharge machining. J Manuf Sci Eng Trans ASME J Manuf Sci Eng Trans ASME 2012;134.

[7] Joshi SN, Pande SS. Thermo-physical modeling of die-sinking EDM process. J Manuf Process 2010;12:45–56.

[8] Murali MS, Yeo S-H. Process Simulation and Residual Stress Estimation of Micro-Electrodischarge Machining Using Finite Element Method. Jpn J Appl Phys 2005;44:5254–63.

[9] Yeo SH, Kurnia W, Tan PC. Electro-thermal modelling of anode and cathode in micro-EDM. J physicsD, Appl Physics 2007;40:2513–21.

[10] Singh A, Ghosh A. A thermo-electric model of material removal during electric discharge machining. Int J Mach Tools Manuf 1999;39:669–82.

[11] Yeo SH, Kurnia W, Tan PC. Critical assessment and numerical comparison of electro-thermal models in EDM. J Mater Process Technol 2008;203:241–51.

[12] Descoeudres a, Hollenstein C, Wälder G, Perez R. Time-resolved imaging and spatially-resolved spectroscopy of electrical discharge machining plasma. J Phys D Appl Phys 2005;38:4066–73.

[13] Shao B, Rajurkar KP, Wu M. Study of Micro-EDM Electro-Thermal Models by Finite Element Method. 9th Int. Conf. MicroManufacturing (ICOMM 2014), 2014.

[14] Xia H, Hashimoto H, Kunieda M, Nishiwaki N. Measurement of energy distribution in continuous EDM process. Journal-Japan Soc Precis … 1996;62:1141–5.

[15] Zahiruddin M, Kunieda M. Energy Distribution Ratio into Micro EDM Electrodes. J Adv Mech Des Syst Manuf 2010;4:1095–106.

[16] Shao B, Rajurkar KP. Micro-EDM Pulse Energy Distribution Ratio Determination. 8th Int. Conf. MicroManufacturing (ICOMM 2013), 2013.

[17] Mills KC. Recommended values of thermophysical properties for selected commercial alloys. Woodhead Publishing; 2002.